Targeting the resolvin E1- eicosapentaenoic acid axis improves hyperinsulinemia and hyperglycemia in a host genetic dependent manner

Anandita Pal[1*], Abrar E. Al-Shaer[1*], William Guesdon[2,], Maria J. Torres[3], Michael Armstrong[4], Kevin Quinn[4], Traci Davis[1], Nichole Reisdorph[4], P. Darrell Neufer[3], Espen E. Spangenburg[3], Ian Carroll[1], Richard P. Bazinet[5], Joan Clària[6] and Saame Raza Shaikh[1]

[1]Department of Nutrition, Gillings School of Public Health and School of Medicine, The University of North Carolina at Chapel Hill; [2]Department of Biochemistry & Molecular Biology, Brody School of Medicine, East Carolina University; [3]Department of Physiology, East Carolina Diabetes & Obesity Institute, East Carolina University; [4]Department of Pharmaceutical Sciences, University of Colorado Denver Anschutz Medical Campus; [5]Department of Nutritional Sciences, University of Toronto; [6]Department of Biomedical Sciences, University of Barcelona, Hospital Clínic-IDIBAPS, Barcelona, Spain.

Present address for William Guesdon: School of Immunology and Microbial Sciences, King's College London
Present address for Maria Torres: Duke Molecular Physiology Institute, Duke University

*both authors contributed equally

Running title: RvE1 and fasting insulin/glucose

Corresponding author: Saame Raza Shaikh, Department of Nutrition, Gillings School of Public Health and School of Medicine, The University of North Carolina at Chapel Hill. shaikhsa@email.unc.edu

The research was supported by: R01AT008375 (SRS), P30DK05635 (SRS), R01AR066660 (ES), NIH/NCRR S10 RR026522-01A1 (NR), R01DK096907 (PDN), Canadian Institutes of Health Research 303157 (RPB) and SAF15-63674-R/2017SGR1449 (JC). This material is also based upon work supported by the National Science Foundation Graduate Research Fellowship Program under Grant No. 1650116 to AEA. Any opinions, findings, and conclusions or recommendations expressed in this material are those of the author(s) and do not necessarily reflect the views of the National Science Foundation. The microbiome studies were supported by the Microbiome Core Facilities, supported in part by NIDDK P30DK34987

Abstract

The insulin/glucose-sensitizing properties of specialized pro-resolving mediators (SPMs) are emerging. We investigated the role of resolvin E1 (RvE1) and its parent molecule eicosapentaenoic acid (EPA) on insulin/glucose homeostasis. We first identified a decrease in the RvE1 precursor 18-hydroxyeicosapentaenoic acid in obese male C57BL/6J mice. Therefore, we investigated the effects of intraperitoneal administration of exogenous RvE1 on obese inbred and outbred male mice. RvE1 administered to obese C57BL/6J mice for just four days improved hyperglycemia and hyperinsulinemia, which was partially dependent on the receptor ERV1/ChemR23. In contrast, RvE1's effects on fasting insulin/glucose were divergent in diversity outbred mice modeling human genetic variation. Next, we studied the preventative effects of pure dietary EPA ethyl esters on obese C57BL/6J mice. EPA ameliorated obesity-induced glucose intolerance, hyperinsulinemia, and hyperglycemia and this was independent from remodeling of the gut microbiome. Supporting analyses of NHANES data revealed that glucose levels were inversely related with EPA intake in obese adults in a sex-specific manner. Finally, secondary SNP analyses revealed extensive genetic variation of human EPA- and RvE1-metabolizing genes. Collectively, the data underscore the importance of the resolvin E1-EPA axis in controlling insulin/glucose homeostasis and point to a therapeutic role for RvE1 that depends on the host genome.

Introduction

Specialized pro-resolving mediators (SPMs) known as lipoxins, resolvins, protectins, and maresins are potent enzymatically-derived metabolites that orchestrate the resolution phase of inflammation and regeneration of damaged tissues [1-4]. SPMs are synthesized predominately from the n-3 polyunsaturated fatty acids (PUFAs) eicosapentaenoic (EPA) and docosahexaenoic acid (DHA)[1]. There is growing evidence from humans and mouse models that obesity impairs the biosynthesis of SPMs and their precursors [5-8]. The loss of SPMs contributes toward a range of obesity-related complications including chronic inflammation, hepatic steatosis, insulin resistance, susceptibility to infection, and delayed wound healing [6,9-14]. Therefore, there is a critical need to understand how specific SPMs and their parent compounds regulate metabolic outcomes in obesity.

The overarching goal of this study was to investigate the role of the SPM resolvin E1 (RvE1) and its parent compound EPA on insulin/glucose homeostasis. The rationale for studying RvE1 was driven by several compelling studies to suggest a potential role for the metabolite in improving metabolic outcomes. For instance, RvE1 administration to genetically obese mice improves adipose tissue expression of adiponectin, GLUT-4, IRS-1 and PPARγ in addition to mitigating hepatic steatosis [9]. Furthermore, overexpression of RvE1's receptor ERV1/ChemR23 improves hyperglycemia and hepatic steatosis of male mice [15]. There is also rigorous evidence that DHA-derived SPMs ameliorate insulin resistance [10,13,16-19]. The DHA-derived SPM protectin D1 alleviates insulin resistance by controlling skeletal muscle IL-6 secretion and resolvin D1 enhances glucose tolerance by targeting adipose tissue macrophage polarization [13,17]. Increased levels of DHA-derived

SPMs and their precursors in fat-1 transgenic mice also protect against obesity-induced insulin resistance [20].

The biosynthesis of endogenous RvE1 is dependent on its parent compound EPA. Circulating levels of EPA are generally low in the western population [21,22]. Therefore, increased intake of EPA is hypothesized to improve metabolic complications related to obesity [23]. However, EPA as a treatment modality to improve insulin resistance and glucose tolerance has routinely failed in clinical trials [24]. In contrast, EPA may have a role in the prevention of obesity-associated insulin resistance [23,24]. Therefore, major limitations in the field of EPA biology need to be addressed. Notably, most preventative studies use levels of EPA that are not achievable in humans; moreover, investigators routinely rely on impure fish oil mixtures of EPA/DHA despite strong evidence that these two fatty acids are structurally and functionally distinct [25,26].

The first objective was to investigate if obesity impairs the levels of EPA-derived metabolites in C57BL/6J mice. We then studied the effects of short-term exogenous administration of RvE1 on hyperinsulinemia and hyperglycemia using C57BL/6J, ERV1/ChemR23 knockout, and diversity outbred (DO) male mice [27]. The knockouts were used to investigate the role of ERV1/ChemR23, the receptor for RvE1, on hyperinsulinemia and hyperglycemia [28]. DO mice are a unique population that model human genetic diversity and were used since the effects of host genetics on SPM biology are largely unknown. We then studied how pure EPA ethyl esters, modeling human pharmacological intake, prevent obesity-induced impairments in hyperglycemia, hyperinsulinemia, and glucose tolerance. Subsequently, we investigated if EPA ethyl esters remodel the composition of the gut microbiome. The rationale for microbiome

studies was driven by evidence that EPA/DHA-enriched fish oils change the composition of gut bacteria to lower systemic inflammation and decrease endotoxemia, a driver of metabolic complications such as insulin resistance [29-31]. Parallel hypothesis-generating metabolomic experiments were conducted to identify targets of EPA ethyl esters. Finally, we conducted select translational studies. Data from the National Health and Nutrition Examination Survey (NHANES) were analyzed to investigate the relationship between glucose levels and dietary intake of PUFAs in a sex-specific manner among obese individuals. We also conducted SNP analyses by mining the Ensembl database to identify genetic variation of EPA and RvE1 metabolizing genes in humans.

Results

Obese male mice have impaired biosynthesis of EPA-derived lipid mediators. We first analyzed the PUFA metabolite lipidome of visceral white adipose tissue (Fig. 1A) and liver (Fig. 1B) of obese male C57BL/6J mice. In both tissues, obesity generally increased select EETs and prostaglandins synthesized from arachidonic acid by ~2-6 fold relative to lean controls. The SPMs 15(R)-LXA4 and LXA4 were respectively increased in adipose tissue (Fig. 1A) and in liver (Fig. 1B). There was no change in LA- or DHA-derived metabolites in either tissue. We observed a dramatic decrease in the EPA-derived metabolites 12-HEPE and 18-HEPE in adipose tissue (Fig. 1C) and liver (Fig. 1D). We also determined if obese female C57BL/6J mice displayed a reduction in EPA-derived metabolites, particularly 18-HEPE. These studies revealed no impairment in the levels of differing HEPEs including 18-HEPE between lean and obese mice for adipose tissue (Suppl. Fig. 1A) and liver (Suppl. Fig. 1B). Overall, the strong reduction of 18-HEPE in male mice set the basis for subsequent experiments with the SPM RvE1, the downstream product of 18-HEPE.

RvE1 improves hyperinsulinemia and hyperglycemia of inbred mice in a manner that is partially dependent on ERV1/ChemR23. The effects of RvE1 were tested on fasting insulin and glucose using canonical inbred C57BL/6J mice. We first studied wild type (WT) littermates and ERV1/ChemR23 knockout (KO) mice to identify the role of ERV1/ChemR23, the receptor for RvE1, on hyperinsulinemia and hyperglycemia. Supplemental Figure 2A and 2B respectively show the experimental scheme and the ERV1/ChemR23 deletion allele. Body composition did not differ between obese WT and

ERV1/Chem23 KO mice administered vehicle control or RvE1 (Fig. 2A). RvE1 improved fasting glucose levels of WT and ERV1/ChemR23 KO mice (Fig. 2B) compared to mice on a high fat diet. Fasting insulin levels were improved in response to RvE1 in WT obese mice but not with ERV1/ChemR23 KO obese mice relative to lean animals (Fig. 2C).

We next determined if the effects of RvE1 on hyperglycemia and hyperinsulinemia were evident with C57BL/6J mice that were purchased obese from Jackson Laboratories, which are generally lower in body weight than our wild type mice. With these mice, we did not conduct a broad lipidomic analysis. However, we measured RvE1 levels via an ELISA and found lower levels of RvE1 in the plasma of obese mice compared to lean controls (Suppl. Fig. 3). RvE1 administration to obese mice had no effect on body weight (Fig. 3D) compared to the mice on a high fat diet. RvE1 restored fasting glucose (Fig. 2E) and improved fasting insulin (Fig. 2F) levels relative to obese mice.

RvE1 does not uniformly improve fasting insulin and fasting glucose of genetically diverse outbred mice. Humans are genetically heterogenous. Therefore, we next asked whether host genetic differences lead to variations in the fasting insulin and fasting glucose response to RvE1. For these studies, we relied on DO mice that model human genetic variability [27]. Administration of a high fat diet for up to 15 weeks led to large variations in body weight. Thus, we used two experimental designs to measure the effects of RvE1 on fasting insulin and fasting glucose. For the first experimental design (Fig. 3A), we administered RvE1 to those mice that exhibited ~14g of fat mass over the course of the period of dietary intervention with a high fat diet. The rationale for selecting ~14g of fat mass was based on the studies with obese C57BL/6J mice (Fig. 2) that were in this range

of fat mass. Body weight gain of the DO mice is depicted in Suppl. Fig. 4A. Relative to baseline, RvE1 improved fasting glucose (Fig. 3B) and fasting insulin (Fig. 3C) levels of approximately half of the obese DO mice. In contrast, using the same experimental design with C57BL/6J mice, fasting glucose (Fig. 3D) and fasting insulin (Fig. 3E) were more uniformly improved in response to RvE1.

A range of DO mice did not attain ~14g of fat mass after 13-15 weeks of consuming a high fat diet. The body weights of these mice are depicted in Suppl. Fig. 4B. With this approach (referred to as the second experimental design, Suppl. Fig. 5A), we obtained the same results as the first experimental design in which nearly half of the DO mice showed an improvement in fasting glucose (Suppl. Fig. 5B) and fasting insulin (Suppl. Fig. 5C), suggesting a critical role for host genetics.

EPA ethyl esters of high purity improve hyperglycemia, hyperinsulinemia, and glucose intolerance of obese male mice. The next set of experiments investigated if dietary administration of pure EPA, the parent compound of RvE1, could prevent obesity-induced metabolic outcomes of obese male mice. The approach relied on pure ethyl esters of EPA and not mixtures of EPA with DHA that can confound the data. We conducted select metabololipidomic studies to ensure that EPA administration was increasing metabolites of the RvE1 pathway. Both 12-HEPE and 18-HEPE levels were strongly elevated (up to 59-fold) in white adipose tissue (Suppl. Fig. 6A) and liver (Suppl. Fig. 6B) upon EPA ethyl ester administration relative to the high fat diet.

Mice consuming a high fat diet in the absence and presence of EPA had similar increases in total mass and fat mass compared to lean controls (Fig. 4A). Inclusion of

EPA in the diet of obese mice improved glucose tolerance (Fig. 4B), as quantified by the area under the curve (Fig. 4C). Relative to the high fat diet, EPA improved fasting glucose (Fig. 4D) and fasting insulin levels (Fig. 4E) and therefore the HOMA-IR score was lowered (Fig 4F). Overall, EPA ethyl esters significantly ameliorated the metabolic insult of the high fat diet.

EPA ethyl ester supplementation does not modify the composition of the gut microbiome relative to mice on a high fat diet. Previous studies suggest that mixtures of EPA/DHA promote specific compositional changes in the microbiome in a manner that supports lower systemic inflammation associated with insulin resistance [29-31]. Therefore, we conducted a microbiome study with control, high fat, and high fat + EPA ethyl ester diets. Using non-metric multidimensional scaling (NMDS) with Bray-Curtis distances, we found a separation in beta diversity between mice fed a control diet verses a high fat or high fat+EPA diet (Fig. 5A). However, the distances between the high fat and high fat+EPA samples were not distinctly defined, indicating little differences in the microbial beta diversity between a high fat diet and high fat+EPA diet. There was little to no change in the relative abundance between high fat and high fat+EPA diets (Fig. 5B). In contrast, the families Erysipelotrichaceae and Lactobacillaceae were decreased between mice consuming high fat diet as compared to control diet. Shannon alpha diversity between mice fed the high fat and high fat+EPA diets were similar (Fig. 5C). The control mice had significantly higher Shannon alpha diversity compared to the EPA-containing diet, suggesting a larger species diversity within the control group. We found the most consistent change between all three dietary groups among the proteobacteria-related

microbes – spanning phylum (Fig. 5D), class (gammaproteobacteria) (Fig. 5E), and order level (betaproteobacteriales) (Fig. 5F). All three proteobacteria-related microbes were elevated between each dietary pairwise comparison. We conducted hierarchal clustering on the samples (Fig. 5G) using the normalized Log10 absolute abundance values and found that the control mice tightly cluster together, whereas the high fat and high fat+EPA samples shared the same parent branch in the dendrogram with little differences between their abundance values. Collectively, these findings suggest that pure EPA ethyl esters do not improve the obesity-driven compositional changes in the gut microbiome.

Metabolomic analyses reveal lipid targets of EPA ethyl esters. Given the mechanism of action for EPA ethyl esters is likely to be pleiotropic, we conducted metabolic profiling of visceral white adipose tissue and liver from mice consuming the experimental diets. Analyses of PCA plots revealed a clear distinction between the control, high fat, and high fat + EPA ethyl ester diets for visceral white adipose (Fig. 6A). EPA ethyl esters were predominately incorporated into triglycerides with some uptake into diglycerides and phosphatidylcholine (Fig. 6B, 6C).

In the liver, PCA plots also showed a clear distinction between the high fat and high fat + EPA ethyl ester diets (Fig. 6D). EPA ethyl esters appeared to have a broad effect on the liver metabolome (Fig. 6E, 6F). EPA acyl chains were likely distributed into triglycerides, phosphatidylcholine, phosphatidylethanolamine, and anandamide (Fig. 6F). Overall, these results showed that EPA ethyl esters are incorporated into several lipid pools, which would then differentially influence metabolic pathways in the adipose tissue

and liver. The full metabolite names, p-values, fold changes, and quantifications are in Supplemental Tables 1 and 2 for the adipose tissue and liver, respectively.

NHANES analyses show glucose levels are inversely related with EPA intake in a sex-specific manner and are also dependent on the ratio of EPA to linoleic acid. We next investigated the relation between EPA intake and blood glucose levels during an OGTT in obese humans. To do so, we analyzed data from NHANES. Increased EPA intake was associated with lower glucose levels between the first and third tertiles for obese males (Fig. 7A) but not females (Fig. 7B). Furthermore, we investigated if there was a relationship between DHA and glucose levels. In obese males (Fig. 7C) and females (Fig. 7D), there was no association between DHA and blood glucose levels.

Metabolites generated from EPA share some of the same enzymes used by n-6 fatty acids such as linoleic acid (LA) [32,33]. Thus, we further mined the NHANES data to determine if there was a relationship between the ratio of LA to EPA on fasting glucose levels. Tertiles of the LA to EPA are plotted for obese men (Fig. 8A) and women (Fig. 8B). The positive association between EPA and glucose levels was diminished and in fact, at the highest ratio of LA to EPA in men (Fig. 8A), but not women (Fig. 8B), blood glucose levels were increased relative to the first two tertiles.

SNP analyses reveal strong genetic variation of human EPA- and RvE1-metabolizing genes. Finally, we investigated if host genetics have a role in the metabolism of EPA and RvE1. Therefore, we mined the Ensembl database containing the dbSNP archive and 1000 genomes data (Suppl. Table 3). We extracted all the CYP450 enzymes that have

the capacity to metabolize EPA, further downstream enzymes leading to the production of E-series resolvins (COX2, ALOX5, FLAP, ALOX12/15, LTA4H), and the two RvE1 receptors (ChemR23 and BLT1) [34-36]. We show a large range of minor allele frequencies where SNPs for each gene are contained in chromosomes 1, 10, 12-15, 17 and 19 with BLT1 lacking SNPs in chromosome 14 (Fig. 9). Genes with lower ranges of minor allele frequencies (MAF) ranging from 0.05 (5%) – 0.38 (38%) include BLT1, COX2, CYP2J2, CYP1A1 and CYP1A2. Surprisingly, all other genes contained many high MAFs with numerous SNPs in the 0.4 (40%) - 0.5 (50%) range (Fig. 9). Moreover, the CYP450 genes contained many SNPs in close proximity (<500 kilobases) on the same chromosome, these include: CYP2C18 and CYP2C19 (~27 Kb apart), CYP2C19 and CYP2C9 (~84 Kb), CYP2C9 and CYP2C8 (~47 Kb), CYPA1A1 and CYPA1A2 (~24 Kb), CYP4F8 and CYP4F3 (~10 Kb), CYP4F3 & CYP4F12 (~10 Kb), and CYP4F12 and CYP4F2 (~181 Kb). Taken together, these results showed high population variance in EPA- and RvE1-metabolizing genes.

Discussion

The data in this manuscript provide valuable information needed for the development of RvE1 as a treatment modality and EPA as a preventative strategy for obesity-associated hyperinsulinemia and hyperglycemia. We first identified that the EPA-derived metabolites 12-HEPE and 18-HEPE are lowered in the adipose tissue and liver of obese male mice. This led us to focus on the therapeutic role of RvE1, a downstream metabolite of 18-HEPE, on hyperglycemia and hyperinsulinemia. We investigated the role of ERV1/ChemR23 and the host genome on the fasting insulin/glucose response to RvE1. Subsequent preventative studies with EPA ethyl esters revealed an improvement in insulin/glucose homeostasis that was independent of a remodeling of the gut microbiome. Finally, we translated some of the findings by conducting secondary analyses of human data, as described below.

A major advancement from this study are data showing that DO mice, which represent human genetic diversity, respond in a divergent manner upon RvE1 administration. The results suggest that RvE1 is unlikely to have a uniform positive effect in all obese humans. Overall, little is known about the role of host genetics on SPM biology. One literature report highlights the importance of host genetics by demonstrating that obese subjects with a C allele in the rs1878022 polymorphism of ERV1/ChemR23 receptor confers protection from adipose tissue inflammation [37]. Further, mining the 1000 genomes and dbSNP databases reveal a large range of MAFs in the EPA and RvE1-metabolizing genes. Most of the genes analyzed reach MAFs close to 50%, indicating large population variance in the EPA/RvE1 pathway. Furthermore, close proximity of the CYP450 enzyme SNPs suggest potential genetic linkage in many of the CYP450 variants

that can potentially influence metabolism of EPA and its downstream metabolites. The results set the basis for future genetics studies that will establish candidate genes regulating the metabolic response to RvE1. This will ultimately aid in establishing 'responders' from 'non-responders' to RvE1 in humans. On the whole, the data highlight the notion that human obesity is highly heterogenous and there is a need for precision administration of therapeutics such as RvE1 based on host genetic profiles.

The functional studies with RvE1 provide strong evidence for further clinical development of RvE1 for improving metabolic outcomes in obesity. There is some ambiguity in the literature regarding the effects of RvE1 on hyperglycemia. Overexpression of ERV1/ChemR23 in myeloid cells improved hyperglycemia and hepatic steatosis of male mice [15]. However, RvE1 administration to wild type mice at a dose of 2ng/g body weight twice weekly for four weeks did not improve hyperglycemia [15]. Our studies relied on a dose of RvE1 (300ng/mouse) for four consecutive days, which may explain the positive effects. Thus, future studies are required to investigate the effects of RvE1 and its mimetics in a dose-dependent manner.

RvE1 is likely exerting its effects through multiple targets and mechanisms. The metabolite rescues hyperglycemia, but not hyperinsulinemia, through ERV1/ChemR23. There is evidence that RvE1 blocks signaling through BLT1, the receptor for the arachidonic acid-derived LTB4 [16]. LTB4 serves as a chemokine for select immune cell populations that exacerbate glucose tolerance [38]. Thus, RvE1 may be inhibiting LTB4 binding to BLT1 to improve chronic inflammation. RvE1 may also be inhibiting signaling through chemerin, an adipokine that binds ERV1/ChemR23 [39]. At the organ and cellular level, RvE1 can improve inflammation though the targeting of intestinal alkaline

phosphatase and specific cell types including neutrophils [14,40,41]. An additional possibility is that RvE1 may exert its effects through the production of its metabolites. This may explain why we did not detect RvE1 in adipose tissue and liver as the SPM may be undergoing increased turnover to oxidized metabolites [6]. Our mass spectrometry assay did not include downstream metabolites like 18-oxo-RvE1. In addition, it is possible that administering other metabolites such as RvE2 or 12-HEPE could further improve outcomes. We did not study the effect of 12-HEPE, which is of particular interest as it was recently identified to improve glucose metabolism [42].

The preventative studies with pure EPA ethyl esters challenge some previous findings in this area of study. Earlies studies have reported a reduction in fat mass with EPA-enriched oils, which we did not observe [43,44]. Perhaps the differences in results lies in the concentration and purity of EPA and the timing as well as duration of intervention. More importantly, EPA did not improve changes in the gut microbiota induced by a high fat diet. Some studies show that n-3 PUFA-enriched fish oils or fat-1 transgenic mice remodel the gut microbiome to lower the abundance of Gram negative bacteria [29-31]. EPA ethyl esters are clearly remodeling several lipid pools (as the metabolomics data show), which may in turn influence metabolites generated by the gut microbiome. Therefore, measuring microbial generated metabolites is an avenue for future investigation with EPA ethyl esters.

The NHANES data highlight the need for preventative precision nutrition studies with EPA. Preventative studies in humans with EPA are generally lacking although one study demonstrated that administration of n-3 PUFAs to healthy human volunteers prevented insulin resistance induced with a glucocorticoid [45]. The NHANES analyses

revealed those subjects with lowest consumption of EPA, but not DHA, had the highest glucose levels in a sex-specific manner. The positive effects of EPA were mitigated when the intake of LA was high. While these data are associative, they point to the importance of discriminating EPA from DHA and importantly accounting for LA levels. LA is of significance for several reasons. LA biosynthesis and metabolism requires some of the same enzymes used for EPA synthesis and metabolism, including the production of downstream metabolites [32,33]. Moreover, LA's consumption in the western diet is 14-18 times the amount required to prevent LA deficiency [22,46] and LA's effects on insulin sensitivity are strongly debated [46-53].

In summary, the results provide strong evidence warranting future studies on how RvE1, and its synthetic analogs, improve metabolic outcomes in obesity and type 2 diabetes in a host-genetic dependent manner. The data also suggest the need for future preventative clinical studies in humans with RvE1's parent compound EPA that would precisely account for background levels of LA, sex-differences and the host genetic profile. These studies will ultimately aid in the prevention and treatment of hyperinsulinemia and hyperglycemia that are associated with obesity.

Materials and Methods

Animal models. C57BL/6J mice of 5-6 weeks of age were fed lean control (10% kcal from lard, Envigo TD.160407) or high fat (60% kcal from lard, Envigo TD.06414) diet in the absence or presence of EPA (Cayman, ≥93%) ethyl esters (Envigo TD.160232) for 15 weeks. EPA in the high fat diet accounted for 2% of total energy [54]. For select studies, C57BL/6J mice were purchased obese from Jackson at 18 weeks of age. They were acclimatized by feeding lean (10% lard, D12450B) or high fat (60% lard, D12492) diets (Research Diets) for an additional 2-3 weeks prior to conducting experiments. DO mice (Jackson) from generation 33 were obtained at 4 weeks of age and acclimated for 2 weeks. The DO population is derived from 144 Collaborative Cross lines obtained from Oak Ridge National Laboratory at generations F4-F12 of inbreeding [27]. DO mice were administered a high fat diet (Envigo) for up to ~14 weeks.

Generation of an ERV1/ChemR23 mutant allele by CRISPR/Cas9-mediated genome editing. Benchling software was used to identify Cas9 guide RNAs flanking the coding sequences of the *Cmklr1 (ERV1/ChemR23)* gene. Three guide RNAs at each end of the target sequence were selected for activity testing. The 5′ and the 3′ guide RNAs were designed to target near the 3′ end of ERV1/ChemR23 intron 2 and the 3′ UTR region after the stop codon in ERV1/ChemR23 exon 3 respectively (Suppl. Fig. 2B, 2C). Guide RNAs were cloned into a T7 promoter vector followed by in vitro transcription and spin column purification. A mouse embryonic fibroblast cell line was transfected with guide RNA and Cas9 protein to perform functional testing. The guide RNA target site was amplified from

transfected cells and analyzed by T7 Endonuclease 1 assay. Guide RNAs selected for genome editing in embryos were 5sg81T (protospacer sequence 5′-GAGATCGTTCACAACCC-3′) and 3sg81T (protospacer sequence 5′-gCGGCCCAGGGACGCCTA-3′). A donor oligonucleotide of sequence 5′-CATACGAATGCAAAATAAAGACAAGAAATGGCAAAAGGGGAGATCGTTCACAATAA TGGGAGACATGCCGGGAGCCTTTGGGAATGCTCCAATGCCCACTGAATTTTG-3′. was included to facilitate homologous recombination to produce a deletion event. However, the founder animal did not have the same deletion junction as the donor oligonucleotide, suggesting the oligonucleotide did not participate in the deletion allele resolution in that founder.

C57BL/6J zygotes were electroporated with 1.2 μM Cas9 protein, 94.5 ng/μl each guide RNA and 400 ng/μl donor oligonucleotide and implanted in recipient pseudopregnant females. Resulting pups were screened by PCR for the presence of a deletion allele. One male founder was identified with a precise deletion between the cut sites of the electroporated guide RNAs. The founder was mated to wild-type C57BL/6J females to establish a colony with the deletion allele. ERV1/ChemR23 animals were detected by PCR with primers Cmklr1-5ScF1 (5′-GGAGCAGGAAACAGAATAGGAC-3′), Cmklr1-3ScF1 (5′-ATCACCTTCTTCCTCTGCTGG-3′) and Cmklr1-3ScR1 (5′-GGTTTGACTGTCATGTTGCCATA-3′). We observe a 580 bp band for the ERV1/ChemR23 deletion allele and a 725 bp band for the ERV1/ChemR23 wild-type allele in this assay.

RvE1 administration**.** RvE1 (Cayman Chemicals) was i.p. administered daily at a concentration of 300ng/100μl in PBS to obese mice for 4 consecutive days. Control mice were administered vehicle control.

Body mass and insulin/glucose measurements. Metabolic studies including Echo-MRI studies were conducted as previously described [8]. Briefly, mice were fasted for 5 hours prior to the establishment of baseline glucose values with a glucometer. For the glucose tolerance test, 2.5g of dextrose (Sigma-Aldrich) per kg lean mass was administered intraperitoneally.

Studies with outbred mice. Since every DO mouse is genetically unique, each mouse served as its own control. Two experimental designs were used with the DO mice. For the first experimental design, baseline fasting insulin/glucose measurements were recorded once each DO mouse achieved ~14 grams of fat mass as measured by Echo-MRI. The mice were then allowed one week to recover and subsequently i.p. injected with 300 ng RvE1 for 4 consecutive days. Fasting glucose and fasting insulin were measured at baseline and 4 days after RvE1 administration. For the second experimental design, DO mice were fed a high fat diet for up to 15 weeks and baseline fasting insulin/glucose measurements were made for those mice that did not reach ~14 grams of fat mass as measured by Echo-MRI. The mice were then allowed one week to recover and subsequently i.p. injected with 300 ng RvE1 for 4 consecutive days. Fasting glucose and fasting insulin were measured at baseline and 4 days after RvE1 administration.

Mass spectrometry-based metabololipidomics. Analyses of PUFA-derived metabolites of visceral white adipose tissue and liver was conducted as previously described [11,55]. Quantitation of lipid mediators was performed using two-dimensional reverse phase HPLC tandem mass spectrometry (liquid chromatography–tandem mass spectrometry). All standards and internal standards used for the LC/MS/MS analysis were purchased from Cayman Chemical (Ann Arbor, Michigan, USA). All solvents and extraction solvents were HPLC grade or better.

Microbiome analyses. DNA from stool was isolated on King Fisher Flex automated instrument using MagMAX™ DNA protocol. Stool samples were transferred to sterile 2 ml tubes containing 200 mg of ≤106µm glass beads (Sigma) and 0.5ml of lysis/binding buffer. Qiagen TissueLyser II was used at 30Hz to carry out bead beating for 3 minutes after which samples were centrifuged at 21000 x g for 3 minutes. Subsequently, 115µl of supernatants were transferred to MME-96 deep well plates followed by addition of magnetic bead mix and isopropanol. Finally, the sample plate was placed into the King Fisher Flex instrument along with two isopropanol-based, two ethanol-based washing solution plates as well as an elution buffer plate and the MME-96 processor script was executed. Upon completion, DNA was stored in elution buffer at -20°C until further processing. 12.5 ng of total DNA was amplified using universal primers targeting the V4 region of the bacterial 16S rRNA gene1, 2. Primer sequences contained overhang adapters appended to the 5′ end of each primer for compatibility with the Illumina sequencing platform. The complete sequences of the primers were:

515F - 5’ TCGTCGGCAGCGTCAGATGTGTATAAGAGACAGGTGCCAGCMGCCGCGGTAA 3’

806R - 5’GTCTCGTGGGCTCGGAGATGTGTATAAGAGACAGGGACTACHVGGGTWTCTAAT 3’.

Master mixes contained 12.5ng of total DNA, 0.2μM of each primer and 2x KAPA HiFi HotStart ReadyMix (KAPA Biosystems). The thermal profile for the amplification of each sample had an initial denaturing step at 95°C for 3 minutes, followed by a cycling of denaturing at 95°C for 30 seconds, annealing at 55°C for 30 seconds, a 30 second extension at 72°C (25 cycles), a 5 minutes extension at 72°C and a final hold at 4°C. Each 16S amplicon was purified using the AMPure XP reagent (Beckman Coulter). In the next step each sample was amplified using a limited cycle PCR program, adding Illumina sequencing adapters and dual-index barcodes (index 1(i7) and index 2(i5)) (Illumina) to the amplicon target. The thermal profile for the amplification had an initial denaturing step at 95°C for 3 minutes, followed by a denaturing cycle of 95°C for 30 seconds, annealing at 55°C for 30 seconds and a 30 second extension at 72°C (8 cycles), a 5 minutes extension at 72°C and a final hold at 4°C. The final libraries were again purified using the AMPure XP reagent (Beckman Coulter), quantified and normalized prior to pooling. The DNA library pool was then denatured with NaOH, diluted with hybridization buffer and heat denatured before loading on the MiSeq reagent cartridge and on the MiSeq instrument. Automated cluster generation and paired–end sequencing with dual reads were performed according to the manufacturer’s instructions.

For analyses, multiplexed paired-end fastq files were produced from the sequencing results of the Illumina MiSeq using the Illumina software conFig.BclToFastq. The paired-end fastq files were joined into a single multiplexed, single-end fastq using the software tool fastq-join. Demultiplexing and quality filtering was performed on the joined results. Quality analysis reports were produced using the FastQC software. Bioinformatics analysis of bacterial 16S amplicon sequencing data was conducted using the Quantitative Insights Into Microbial Ecology (QIIME2) software. DADA2 was used for denoising, removal of chimeric sequences, and construction of amplicon sequence variants (ASVs). Feature classification was preformed using the SILVA database in the QIIME2 Naïve Bayes classifier (silva-132-99-nb-classifier). Shannon alpha diversity was calculated using the QIIME2 q2-diversity plugin and beta diversity was calculated utilizing non-metric multidimensional scaling (NMDS) with Bray-Curtis distances. All feature tables generated by the QIIME2 software were imported into the Phyloseq R package and normalized via DESeq2.

Untargeted metabolomics. Adipose tissue and liver were homogenized using a bead homogenizer and prepared for metabolomics using previously described methods [56]. Samples were analyzed using liquid chromatography mass spectrometry (LCMS) and raw data were extracted and processed using Agilent Technologies Mass Hunter Profinder Version B.08.00 (Profinder) software in combination with Agilent Technologies Mass Profiler Professional Version 14 (MPP) as previously described [56-58]. An in-house database containing METLIN, Lipid Maps, Kyoto Encyclopedia of Genes and Genomes (KEGG), and Human Metabolomics Database (HMDB) was used to annotate metabolites based on exact mass, isotope ratios, and isotopic distribution with a mass error cutoff of

10 ppm. This corresponds to annotation at Metabolomics Standards Initiative (MSI) level 3 [59].

To visualize clustering between the dietary groups we ran a principal component analysis (PCA) using all metabolites. We then determined statistically significant metabolites between obese mice and obese mice supplemented with EPA. One of the samples from the high fat diet (HF_105) was an outlier from all the other samples and was excluded from analyses. We then calculated fold changes (EPA/high fat). Next, using the validated significant metabolites with Log2 fold changes ±1.5 we standardized the abundances of the metabolites by assigning a Z-score for each sample based on the distribution of the given metabolite. We utilized the Z-scores to generate heatmaps annotated with the classification of each metabolite.

NHANES analyses. The 2013-2014 NHANES database was mined for daily average intake of PUFAs with respect to age, sex, and BMI. We used Rv3.4.4 with the RNHANES package to retrieve the NHANES database. Graphical packages ggpubr and ggplot2 were used to generate all graphs and statistical annotations. The “Dietary Interview - Total Nutrient Intakes” section of the NHANES database was used to retrieve PUFA intake measurements based on a 24-hour dietary recall questionnaire. OGTT 2-hour glucose measurements were retrieved from the “Current Health Status” section, where BMI was retrieved from “Body Measures”. Tertiles of PUFA intake were calculated corresponding to the probability of intake at 33.3%, 67%, and 100% of the range. Normality and homogeneity of variance were tested with the Shapiro-Wilks test and Bartlett test respectively. The dataset did not satisfy the assumptions of normality and

heteroscedasticity; therefore, we utilized a Kruskal-Wallis test followed by a Wilcoxon pairwise test to measure significant differences between tertiles of PUFA intake.

SNP analyses. We used the Biomart tool to mine the Ensembl Variation 98 Human Short Variants (GRCh38.p13) database for single nucleotide polymorphisms (SNPs) with minor allele frequencies at or above 5% that are contained within the 1000 genomes project or the NCBI dbSNP archive. We mined SNPs in the following genes: PTGS2/COX2 (ENSG00000073756), CYP1A1 (ENSG00000140465), CYP1A2 (ENSG00000140505), CYP2E1 (ENSG00000130649), CYP2C8 (ENSG00000138115), CYP2C9 (ENSG00000138109), CYP2C18 (ENSG00000108242), CYP2C19 (ENSG00000165841), CYP2J2 (ENSG00000134716), CYP4F2 (ENSG00000186115), CYP4F3 (ENSG00000186529), CYP4F8 (ENSG00000186526), CYP4F12 (ENSG00000186204), CYP2S1 (ENSG00000167600), CMKLR1/ChemR23 (ENSG00000174600), LTB4R/BLT1 (ENSG00000213903), ALOX12/15 (ENSG00000108839 & ENSG00000161905), ALOX5 (ENSG00000012779), ALOX5AP/FLAP (ENSG00000132965), LTA4H (ENSG00000111144). We used the ggplot2 package in R v3.4.4 to plot all the minor allele frequencies by each allele for every gene and chromosome. White lines in the graph represent a break/gap in the minor allele frequency (MAF) distribution, for example a gene may contain MAFs ranging from 0.05-1.5 then 2.5-4.5 with a “break” between the 1.5-2.5 gap. The distances between the SNPs of different genes on the chromosomes was determined using the base pair location at the last SNP of the first gene and the first SNP of the second gene. Distances below 500

kilobases were considered as having a higher likelihood for genetic linkage, as described by the HapMap project Haploview tool.

Statistics. Data were analyzed using Graph Pad Prism Version 7.0. Lipidomic studies relied on a two-tailed t test. Statistical significance for other analyses relied on one-way or two-way ANOVAs followed by a post-hoc Tukey multiple comparison tests. Most data sets displayed normalized distribution as determined by a Kolmogorov-Smirnov test. Those data sets that did not display normalized distributions were analyzed with a Kruskal-Wallis test followed by a Dunn's multiple comparison test or Wilcoxon pairwise test. Studies as a function of time were analyzed with a two-way ANOVA. For clarity, additional description of analyses for microbiome, metabolomics, and NHANES datasets are included with each corresponding methods section above. For all analyses, $p<0.05$ was considered statistically significant.

Study approval. All murine experiments adhered to IACUC guidelines established by The University of North Carolina at Chapel Hill and East Carolina University for euthanasia and humane treatment.

Figure Legends

Figure 1. Obese male C57BL/6J mice have impaired levels of EPA-derived 12-HEPE and 18-HEPE. Mass spectrometry based metabololipidomic analyses of (A) visceral white adipose tissue and (B) liver. Metabolites from eicosapentaenoic acid (EPA), docosahexaenoic acid (DHA), linoleic acid (LA) and arachidonic acid (AA) are depicted in the heat map. Male mice consumed experimental diets for 15 weeks. N=4-5 mice per diet. Data are average ± S.D. *p<0.05, **p<0.01, ***p<0.001 by a two-tailed t test.

Figure 2. Short-term administration of RvE1 to inbred mice improves obesity-driven impairments in fasting glucose and fasting insulin partially mediated by the receptor ERV1/ChemR23. (A) Body weight (B) fasting glucose and (C) fasting insulin levels of male wild type (WT) and ERV1/ChemR23 knockout (KO) mice consuming a lean control diet (Con) or high fat (HF) diet in the absence or presence of RvE1. Corresponding (D) body weight, (E) fasting glucose and (F) fasting insulin levels of C57BL/6J male mice purchased as obese from Jackson Laboratories. All measurements were made at 13-14 weeks of dietary intervention. N=6-7 mice per diet (A-C), N=14 mice per diet (D-F). Values are means ± SD. *p<0.05, **p<0.01, ***p<0.001, ****p<0.0001 by one-way ANOVA followed by Tukey's multiple comparisons test.

Figure 3. Obese diversity outbred mice display a differential response to fasting glucose and fasting insulin upon exogenous RvE1 administration. (A) Schematic representation of study design. Fasting glucose and insulin measurements were obtained prior to (baseline) and after 4 days of RvE1 administration. Only those DO male mice that

were ~14 grams of fat mass were used for these studies. (B) Fasting glucose and (C) fasting insulin levels after a 5 hour fast. Corresponding studies with C57BL/6J mice using the same experimental design of intervention are depicted for (D) fasting glucose and (E) fasting insulin. All data are plotted as the fold change in glucose and insulin relative to baseline. N =19 DO mice and N= 6 C57BL/6J mice. **p<0.01 by a paired two-tailed t test.

Figure 4. EPA ethyl esters prevent obesity-induced impairments in glucose tolerance, fasting glucose and fasting insulin levels of C57BL/6J mice. (A) Body composition measured by Echo-MRI. (B) Glucose tolerance test performed by intraperitoneal injection of glucose after a 5 hour fast. (C) Area under the curve (AUC), calculated by integration of the curves in B normalized to baseline values. (D) Fasting glucose and (E) fasting insulin levels after a 5 hour fast. (F) HOMA-IR scores. For all measurements, male mice consumed a lean control diet (Con), a high fat (HF) diet, or a HF diet supplemented with EPA ethyl esters. Measurements were conducted at week 13 of intervention. Values are means ± SD. *p<0.05, **p<0.01, ***p<0.001, ****p<0.0001 from one-way ANOVA followed by Tukey's multiple comparisons test except B, which was a two-way ANOVA followed by a post hoc test.

Figure 5. EPA ethyl esters do not improve obesity-driven modifications to the gut microbiome. C57BL/6J male mice consumed a control (Con), high fat (HF) and HF+EPA ethyl ester diet. (A) NMDS plot with Bray-Curtis distances portraying beta-diversity between samples. (B) Family level relative abundances calculated from normalized absolute abundances. (C) Shannon alpha diversity between diet groups calculated by QIIME2. (D) Log10 normalized absolute abundance of phylum level proteobacteria. (E)

Log10 normalized absolute abundance of class level gammaproteobacteria. (F) Log10 normalized absolute abundance of order level betaproteobacteriales. (G) Heatmap of Log10 normalized absolute abundances with hierarchal complete linkage clustering of the taxa (columns) and samples (rows). Values are means ± SD; *p<0.05, **p<0.01, ***p<0.001 from Wilcoxon pairwise test. n=8-11 mice per diet.

Figure 6. Metabolomic profiling reveals a broad distribution of EPA in white adipose tissue and liver of obese C57BL/6J male mice. C57BL/6J male mice consumed a control (Con), high fat (HF) and HF+EPA ethyl ester diet. (A) PCA plot of validated adipose tissue metabolites between control, HF, and HF+EPA samples. (B) Heatmap of Z-scores from significant adipose tissue metabolites with ±1.5 fold-change. (C) Log2 fold change graph of EPA-containing (20:5) adipose metabolites. (D) PCA plot of validated liver metabolites between control, HF, and HF+EPA samples. (E) Heatmap of Z-scores from significant liver metabolites with ±1.5 fold-change. (F) Log2 fold change graph of EPA-containing (20:5) adipose metabolites. Heatmap legends on the right hand side of (B) and (E) show each metabolite's classifications: triglyceride (TG), diacylglycerol (DG), phosphatidylethanolamine (PE), lysophosphatidylethanolamine (LysoPE), phosphatidic acid (PA), phosphatidylcholine (PC), phosphatidylserine (PS), phosphatidylglycerol (PG), phosphatidylinositol (PI), arachidonoylethanolamine (AEA), cholesterol (CL), and docosahexaenoic acid (DHA). Full metabolite names are provided in the supplemental.

Figure 7. Glucose levels are inversely related to EPA intake in obese men but not women. NHANES data on two-hour glucose measurements (mg/dl) from an OGTT were stratified by tertiles of EPA intake in grams for obese (A) males and (B) females. DHA intake is also depicted for (C) males and (D) females. The range of EPA intake for males was 0.0-0.009g for tertile 1, 0.01-0.068g for tertile 2, 0.069g and above for tertile 3. For females, the intake is 0-0.009 for tertile 1, 0.01-1.51g for tertile 2, 1.52g and above for tertile 3. The range of DHA intake for males is 0.01-0.05g for tertile 1, 0.06-1.49g for tertile 2, and 1.5g and above for tertile 3. The range of DHA intake for females was 0.01-0.03g for tertile 1, 0.04-2.35g for tertile 2, and 2.36g and above for tertile 3. Subjects were adults (18 years and older) and had a BMI of 30 and above. Values are means ± SEM; *$p<0.05$, **$p<0.01$ from Wilcoxon pairwise test. Number of subjects for each tertile is listed on the x-axis.

Figure 8. A high linoleic acid to EPA ratio is associated with an elevation in blood glucose in obese males but not females. Tertiles of the ratio of LA to EPA are presented for obese (A) males and (B) females. The tertiles correspond to 33%, 67%, and 100% of the range of LA to EPA intake for subjects older than 18 and a BMI of 30 and above. *$p<0.05$, **$p<0.001$. Values are means ± SEM; *$p<0.05$, **$p<0.01$ from Wilcoxon pairwise test. Number of subjects for each tertile is listed on the x-axis.

Figure 9. SNPs in EPA and RvE1 metabolizing genes. Data mined from the 1000 genomes and dbSNP human variants databases shows SNPs in the EPA and RvE1

metabolizing genes stratified by each minor allele (A,C,G,T). The SNPs in each gene are plotted by minor allele frequencies and the chromosome that contains the SNP.

Author contributions. A.P. designed and conducted experiments, wrote the manuscript, analyzed data; A.E.A. designed and conducted experiments, wrote parts of the manuscript, analyzed data; W.G. designed and conducted experiments, analyzed data; M.T. conducted experiments; M.A. conducted experiments and analyzed data; K.Q. conducted experiments and analyzed data; T.D. conducted experiments; N.R. designed experiments and provided intellectual input on select analyses; P.D.N. designed experiments; E.E.S. conducted and designed experiments and provided intellectual input on select experiments; I.C. designed experiments and analyzed data; R.B. designed experiments and analyzed data; J. C. provided intellectual input on select data sets and contributed toward editing, and S.R.S. designed experiments, analyzed data, wrote parts of the manuscript and directed the overall research.

Acknowledgements. We thank Dr. Dale Cowley from the UNC Animal Models Core for his assistance in generating the ERV1/ChemR23 KO mice and UNC's Microbiome Core Facilities.

Conflict of Interest: RPB has received industrial grants, including those matched by the Canadian government, and/or travel support related to work on brain fatty acid uptake from Arctic Nutrition, Bunge Ltd., DSM, Fonterra, Mead Johnson, Nestec Inc., and Pharmavite. Moreover, RPB is on the executive of the International Society for the Study

of Fatty Acids and Lipids and held a meeting on behalf of Fatty Acids and Cell Signaling, both of which rely on corporate sponsorship. RPB has given expert testimony in relation to supplements and the brain. SRS has received industry grants including research related to n-3 fatty acids from GSK and Organic Technologies.

References

1. Serhan CN, Levy BD. Resolvins in inflammation: emergence of the pro-resolving superfamily of mediators. *J Clin Invest.* 2018;128(7):2657-2669.
2. Serhan CN. Pro-resolving lipid mediators are leads for resolution physiology. *Nature.* 2014;510(7503):92-101.
3. Serhan CN, Chiang N, Dalli J. New pro-resolving n-3 mediators bridge resolution of infectious inflammation to tissue regeneration. *Molecular Aspects of Medicine.* 2018;64:1-17.
4. Serhan CN, de la Rosa X, Jouvene C. Novel mediators and mechanisms in the resolution of infectious inflammation: evidence for vagus regulation. *J Intern Med.* 2019;286(3):240-258.
5. Lopez-Vicario C, et al. Leukocytes from obese individuals exhibit an impaired SPM signature. *FASEB J.* 2019;33(6):7072-7083.
6. Clària J, Dalli J, Yacoubian S, Gao F, Serhan CN. Resolvin D1 and Resolvin D2 Govern Local Inflammatory Tone in Obese Fat. *J Immunol.* 2012;189(5):2597-2605.
7. Neuhofer A, et al. Impaired local production of proresolving lipid mediators in obesity and 17-HDHA as a potential treatment for obesity-associated inflammation. *Diabetes.* 2013;62(6):1945-1956.
8. Crouch MJ, et al. Frontline Science: A reduction in DHA-derived mediators in male obesity contributes toward defects in select B cell subsets and circulating antibody. *J Leukoc Biol.* 2019;106(2):241-257.

9. González-Périz A, et al. Obesity-induced insulin resistance and hepatic steatosis are alleviated by ω-3 fatty acids: a role for resolvins and protectins. *FASEB J.* 2009;23(6):1946-1957.

10. Titos E, et al. Signaling and immunoresolving actions of resolvin D1 in inflamed human visceral adipose tissue. *J Immunol.* 2016;197(8):3360-3370.

11. Kosaraju R, et al. B cell activity is impaired in human and mouse obesity and is responsive to an essential fatty acid upon murine influenza infection. *J Immunol.* 2017;198(12):4738-4752.

12. Tang Y, Zhang MJ, Hellmann J, Kosuri M, Bhatnagar A, Spite M. Proresolution therapy for the treatment of delayed healing of diabetic wounds. *Diabetes.* 2013;62(2):618-627.

13. Hellmann J, Tang Y, Kosuri M, Bhatnagar A, Spite M. Resolvin D1 decreases adipose tissue macrophage accumulation and improves insulin sensitivity in obese-diabetic mice. *FASEB J.* 2011;25(7):2399-2407.

14. Freire MO, Dalli J, Serhan CN, Van Dyke TE. Neutrophil resolvin E1 receptor expression and function in Type 2 diabetes. *J Immunol.* 2017;198(2):718-728.

15. Sima C, et al. ERV1 Overexpression in myeloid cells protects against high fat diet induced obesity and glucose intolerance. *Scientific Reports.* 2017;7(1):12848.

16. Sima C, Paster B, Van Dyke TE. Function of pro-resolving lipid mediator resolvin E1 in type 2 diabetes. *Crit Rev Immunol.* 2018;38(5):343-365.

17. White PJ, et al. Protectin DX alleviates insulin resistance by activating a myokine-liver glucoregulatory axis. *Nat Med.* 2014;20(6):664-669.

18. Jung TW, Kim HC, Abd El-Aty AM, Jeong JH. Protectin DX ameliorates palmitate- or high-fat diet-induced insulin resistance and inflammation through an AMPK-PPARalpha-dependent pathway in mice. *Sci Rep.* 2017;7(1):1397.

19. Jung TW, et al. Protectin DX ameliorates palmitate-induced hepatic insulin resistance through AMPK/SIRT1-mediated modulation of fetuin-A and SeP expression. *Clin Exp Pharmacol Physiol.* 2019;46(10):898-909.

20. White PJ, Arita M, Taguchi R, Kang JX, Marette A. Transgenic restoration of long-chain n-3 fatty acids in insulin target tissues improves resolution capacity and alleviates obesity-linked inflammation and insulin resistance in high-fat–fed mice. *Diabetes.* 2010;59(12):3066-3073.

21. Stark KD, Van Elswyk ME, Higgins MR, Weatherford CA, Salem N, Jr. Global survey of the omega-3 fatty acids, docosahexaenoic acid and eicosapentaenoic acid in the blood stream of healthy adults. *Prog Lipid Res.* 2016;63:132-152.

22. Blasbalg TL, Hibbeln JR, Ramsden CE, Majchrzak SF, Rawlings RR. Changes in consumption of omega-3 and omega-6 fatty acids in the United States during the 20th century. *Am J Clin Nutr.* 2011;93(5):950-962.

23. Lalia AZ, Lanza IR. Insulin-Sensitizing Effects of Omega-3 Fatty Acids: Lost in Translation? *Nutrients.* 2016;8(6):329.

24. Brown TJ, et al. Omega-3, omega-6, and total dietary polyunsaturated fat for prevention and treatment of type 2 diabetes mellitus: systematic review and meta-analysis of randomised controlled trials. *BMJ.* 2019;366:l4697.

25. Leng X, et al. All n-3 PUFA are not the same: MD simulations reveal differences in membrane organization for EPA, DHA and DPA. *Biochim Biophys Acta Biomembr.* 2018;1860(5):1125-1134.

26. Klingel SL, et al. EPA and DHA have divergent effects on serum triglycerides and lipogenesis, but similar effects on lipoprotein lipase activity: a randomized controlled trial. *Am J Clin Nutr.* 2019.

27. Churchill GA, Gatti DM, Munger SC, Svenson KL. The Diversity Outbred mouse population. *Mamm Genome.* 2012;23(9-10):713-718.

28. Arita M, Ohira T, Sun YP, Elangovan S, Chiang N, Serhan CN. Resolvin E1 selectively interacts with leukotriene B4 receptor BLT1 and ChemR23 to regulate inflammation. *J Immunol.* 2007;178(6):3912-3917.

29. Kaliannan K, Wang B, Li XY, Kim KJ, Kang JX. A host-microbiome interaction mediates the opposing effects of omega-6 and omega-3 fatty acids on metabolic endotoxemia. *Sci Rep.* 2015;5:11276.

30. Caesar R, Tremaroli V, Kovatcheva-Datchary P, Cani PD, Backhed F. Crosstalk between gut microbiota and dietary lipids aggravates WAT inflammation through TLR signaling. *Cell Metab.* 2015;22(4):658-668.

31. Bidu C, et al. The transplantation of omega3 PUFA-altered gut microbiota of fat-1 mice to wild-type littermates prevents obesity and associated metabolic disorders. *Diabetes.* 2018;67(8):1512-1523.

32. Choque B, Catheline D, Rioux V, Legrand P. Linoleic acid: between doubts and certainties. *Biochimie.* 2014;96:14-21.

33. Innes JK, Calder PC. Omega-6 fatty acids and inflammation. *Prostaglandins Leukot Essent Fatty Acids.* 2018;132:41-48.

34. Westphal C, Konkel A, Schunck WH. CYP-eicosanoids--a new link between omega-3 fatty acids and cardiac disease? *Prostaglandins Other Lipid Mediat.* 2011;96(1-4):99-108.

35. Fer M, et al. Metabolism of eicosapentaenoic and docosahexaenoic acids by recombinant human cytochromes P450. *Arch Biochem Biophys.* 2008;471(2):116-125.

36. Fromel T, et al. Cytochrome P4502S1: a novel monocyte/macrophage fatty acid epoxygenase in human atherosclerotic plaques. *Basic Res Cardiol.* 2013;108(1):319.

37. Lopez-Vicario C, et al. Association of a variant in the gene encoding for ERV1/ChemR23 with reduced inflammation in visceral adipose tissue from morbidly obese individuals. *Sci Rep.* 2017;7(1):15724.

38. Li P, et al. LTB4 promotes insulin resistance in obese mice by acting on macrophages, hepatocytes and myocytes. *Nat Med.* 2015;21(3):239-247.

39. Mariani F, Roncucci L. Chemerin/chemR23 axis in inflammation onset and resolution. *Inflam Res.* 2015;64(2):85-95.

40. Campbell EL, et al. Resolvin E1-induced intestinal alkaline phosphatase promotes resolution of inflammation through LPS detoxification. *Proc Natl Acad Sci USA.* 2010;107(32):14298-14303.

41. Herrera BS, et al. Impact of resolvin E1 on murine neutrophil phagocytosis in type 2 diabetes. *Infect Immun.* 2015;83(2):792-801.

42. Leiria LO, et al. 12-Lipoxygenase regulates cold adaptation and glucose metabolism by producing the omega-3 lipid 12-HEPE from brown fat. *Cell Metab.* 2019;30(4):768-783 e767.

43. Pinel A, et al. EPA prevents fat mass expansion and metabolic disturbances in mice fed with a Western diet. *J Lipid Res.* 2016;57(8):1382-1397.

44. Pahlavani M, et al. Eicosapentaenoic acid regulates brown adipose tissue metabolism in high-fat-fed mice and in clonal brown adipocytes. *J Nutr Biochem.* 2017;39:101-109.

45. Delarue J, Li CH, Cohen R, Corporeau C, Simon B. Interaction of fish oil and a glucocorticoid on metabolic responses to an oral glucose load in healthy human subjects. *Br J Nutr.* 2006;95(2):267-272.

46. Naughton SS, Mathai ML, Hryciw DH, McAinch AJ. Linoleic acid and the pathogenesis of obesity. *Prostaglandins Other Lipid Mediat.* 2016;125:90-99.

47. Jandacek RJ. Linoleic Acid: A Nutritional Quandary. *Healthcare (Basel).* 2017;5(2).

48. Whelan J, Fritsche K. Linoleic acid. *Adv Nutr.* 2013;4(3):311-312.

49. Wu JHY, et al. Omega-6 fatty acid biomarkers and incident type 2 diabetes: pooled analysis of individual-level data for 39 740 adults from 20 prospective cohort studies. *Lancet Diabetes Endocrinol.* 2017;5(12):965-974.

50. Zong G, et al. Associations between linoleic acid intake and incident type 2 diabetes among U.S. men and women. *Diabetes Care.* 2019;42(8):1406-1413.

51. Henderson G, Crofts C, Schofield G. Linoleic acid and diabetes prevention. *Lancet Diabetes Endocrinol.* 2018;6(1):12-13.

52. Mamounis KJ, Yasrebi A, Roepke TA. Linoleic acid causes greater weight gain than saturated fat without hypothalamic inflammation in the male mouse. *J Nutr Biochem.* 2017;40:122-131.

53. Oosting A, Kegler D, van de Heijning BJ, Verkade HJ, van der Beek EM. Reduced linoleic acid intake in early postnatal life improves metabolic outcomes in adult rodents following a Western-style diet challenge. *Nutr Res.* 2015;35(9):800-811.

54. Teague H, Harris M, Fenton J, Lallemand P, Shewchuk B, Shaikh SR. Eicosapentaenoic and docosahexaenoic acid ethyl esters differentially enhance B-cell activity in murine obesity. *J Lipid Res.* 2014; 55:1420-1433.

55. Sullivan EM, et al. Murine diet-induced obesity remodels cardiac and liver mitochondrial phospholipid acyl chains with differential effects on respiratory enzyme activity. *J Nutr Biochem.* 2017;45:94-103.

56. Yang Y, Cruickshank C, Armstrong M, Mahaffey S, Reisdorph R, Reisdorph N. New sample preparation approach for mass spectrometry-based profiling of plasma results in improved coverage of metabolome. *J Chromatogr A.* 2013;1300:217-226.

57. Cruickshank-Quinn CI, et al. Transient and persistent metabolomic changes in plasma following chronic cigarette smoke exposure in a mouse model. *PLoS One.* 2014;9(7):e101855.

58. Quinn KD, et al. Dysregulation of metabolic pathways in a mouse model of allergic asthma. *Allergy.* 2017;72(9):1327-1337.

59. Sumner LW, et al. Proposed minimum reporting standards for chemical analysis Chemical Analysis Working Group (CAWG) Metabolomics Standards Initiative (MSI). *Metabolomics.* 2007;3(3):211-221.

60. Arita M, et al. Metabolic inactivation of resolvin E1 and stabilization of its anti-inflamamtory actions. *J Biol Chem.* 2006;281:22847-22854.

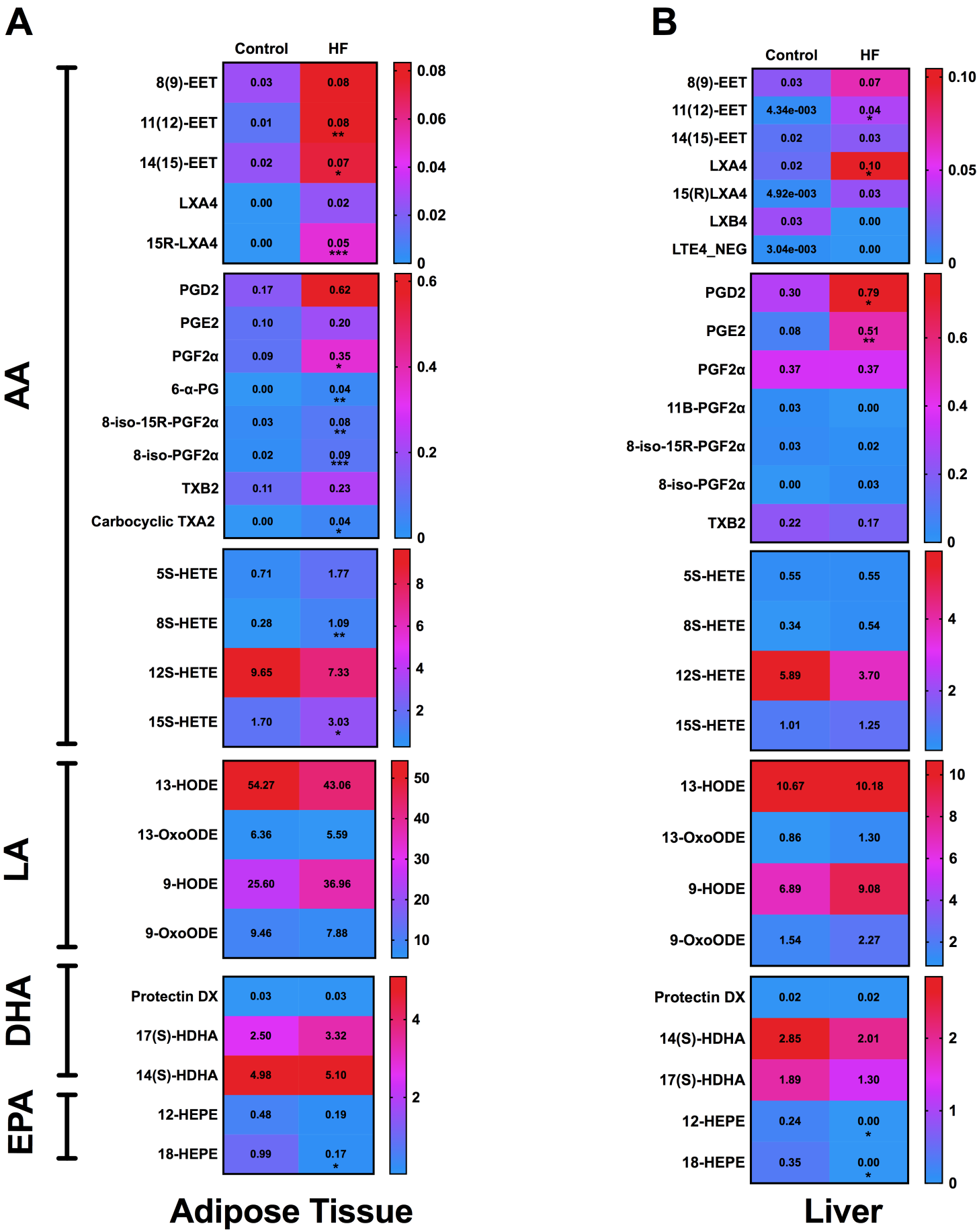

Figure 1

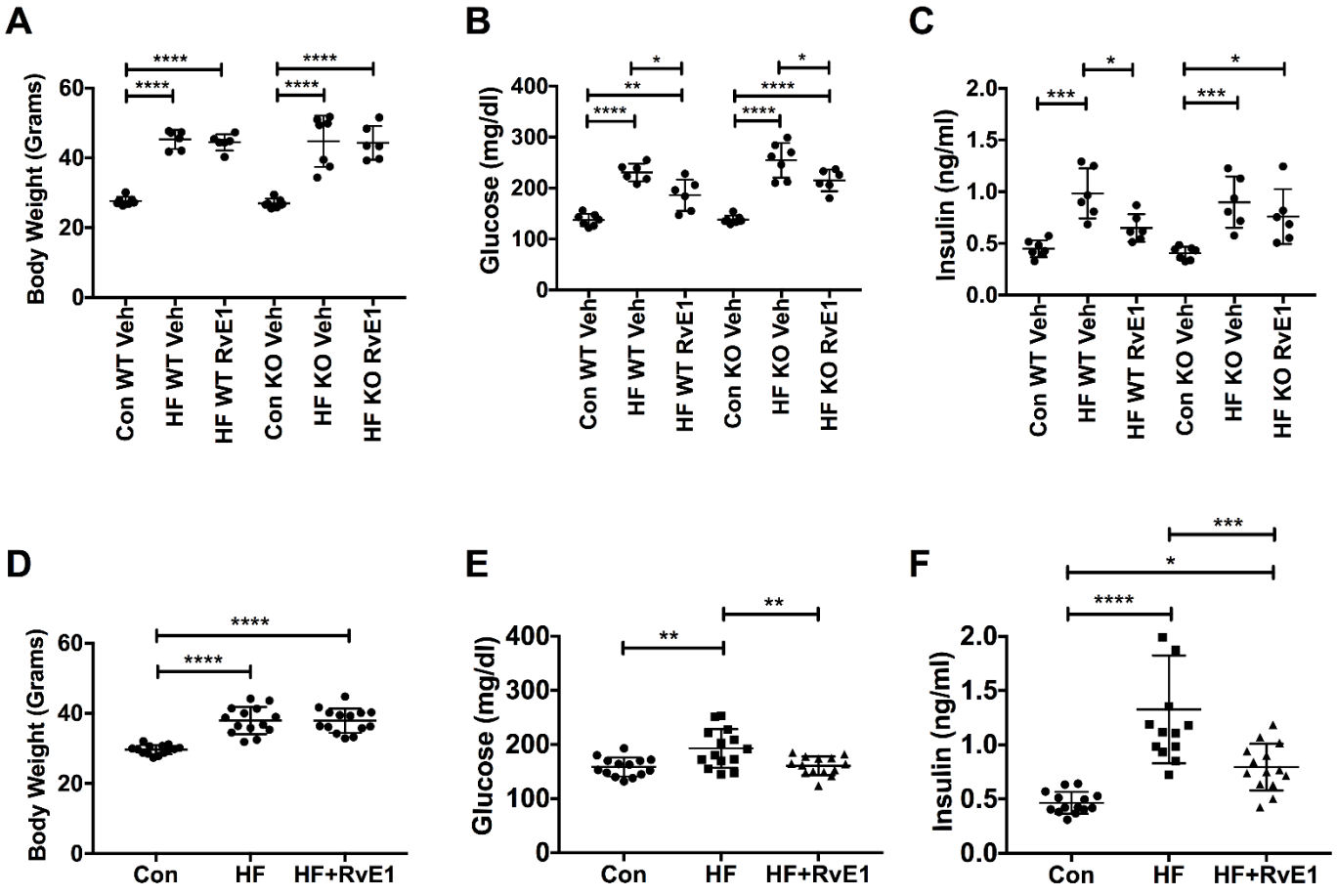

Figure 2

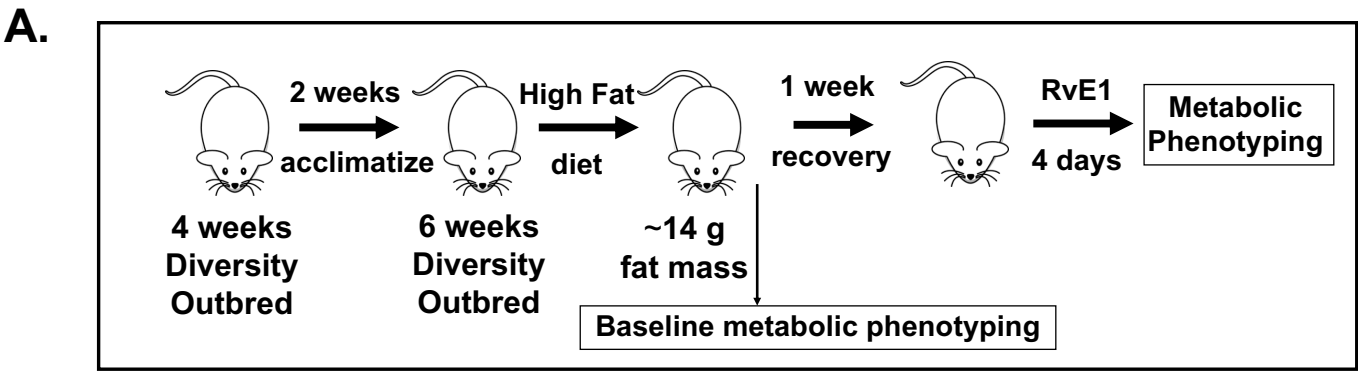

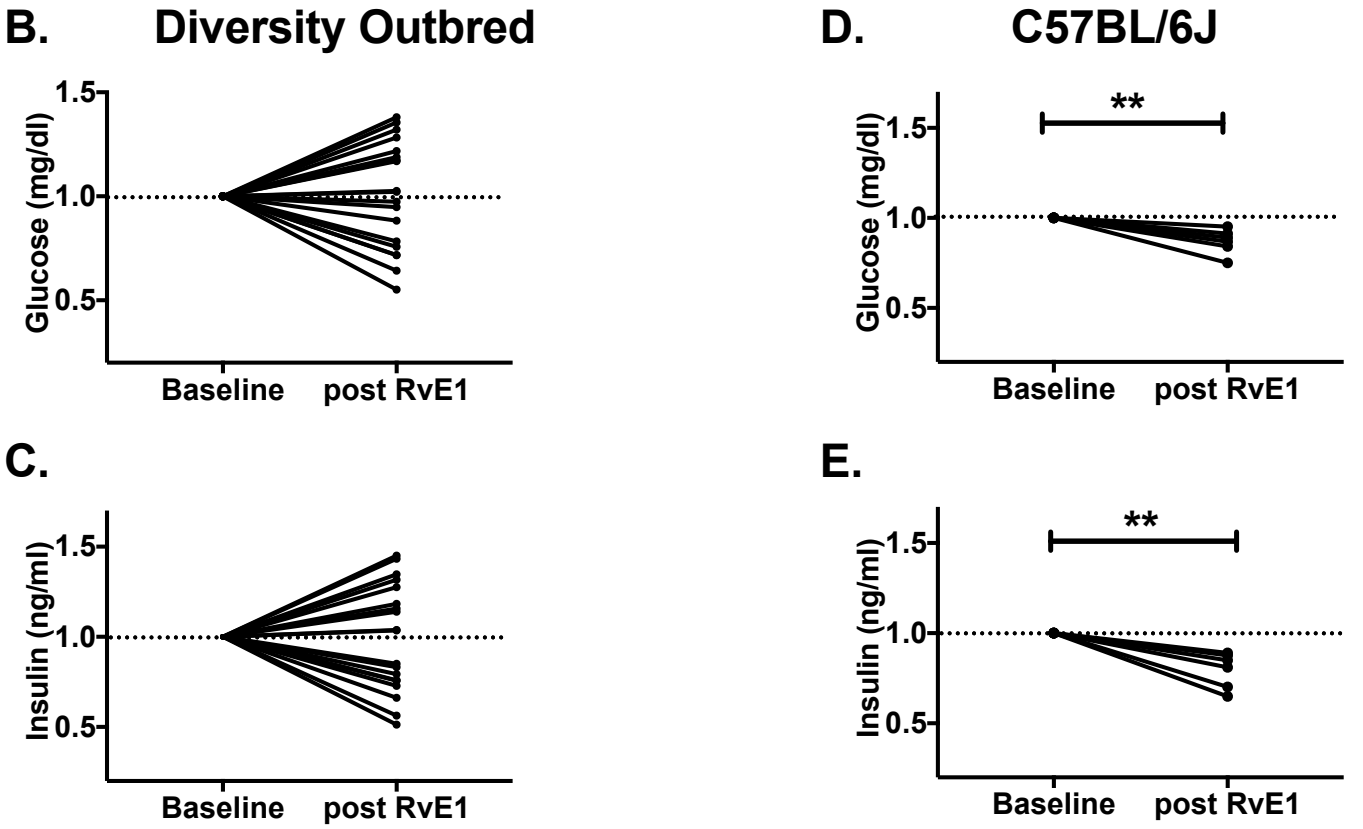

Figure 3

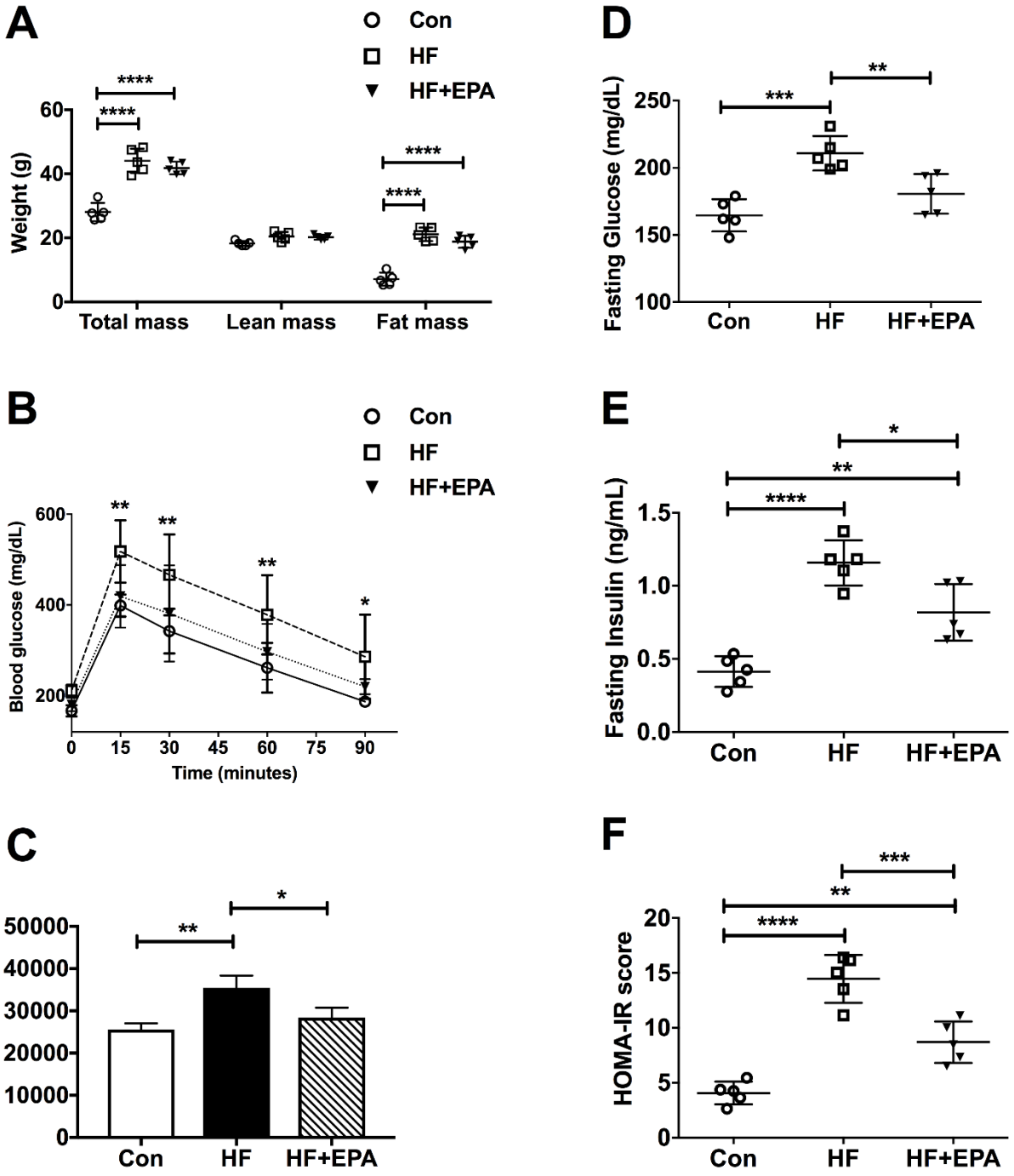

Figure 4

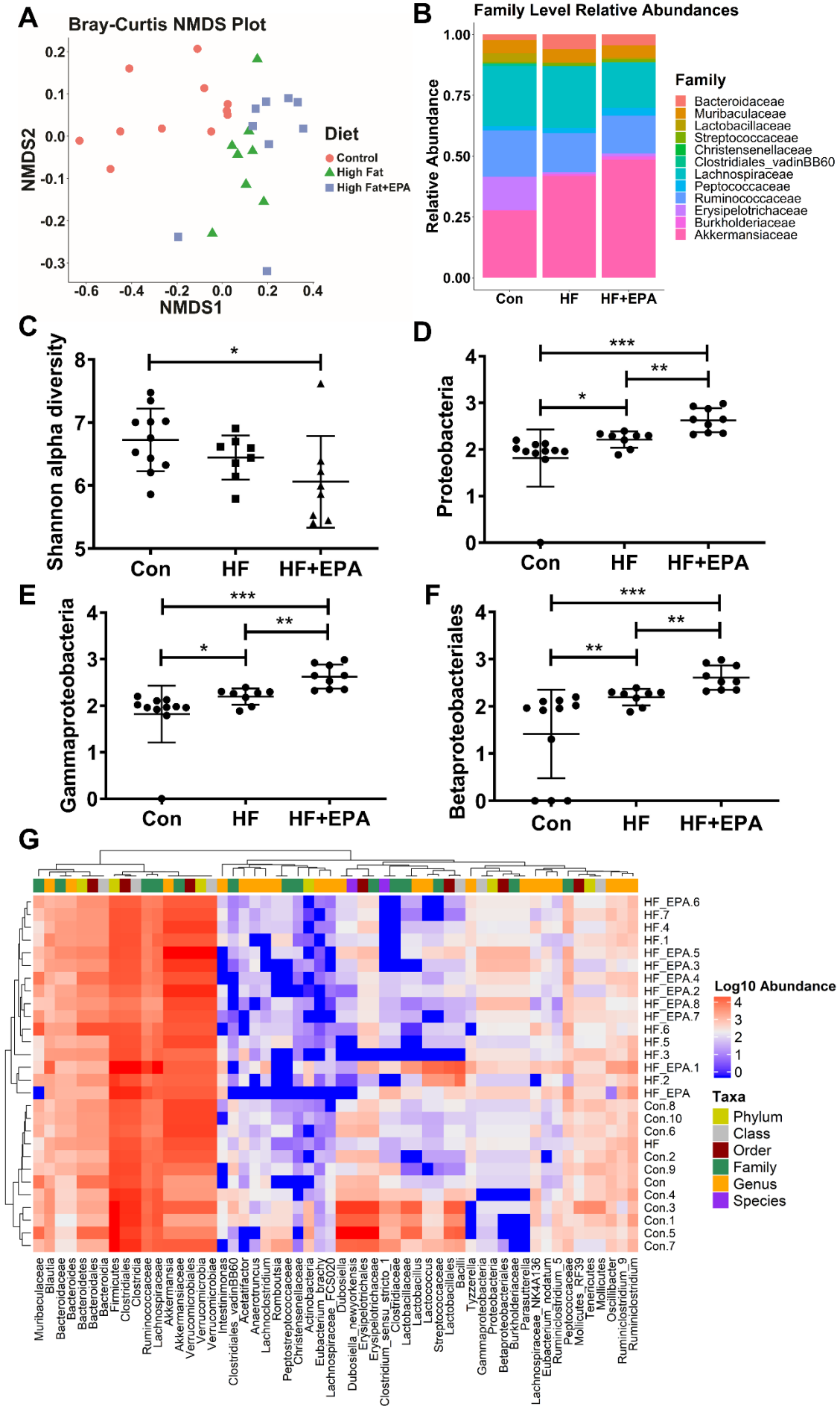

Figure 5

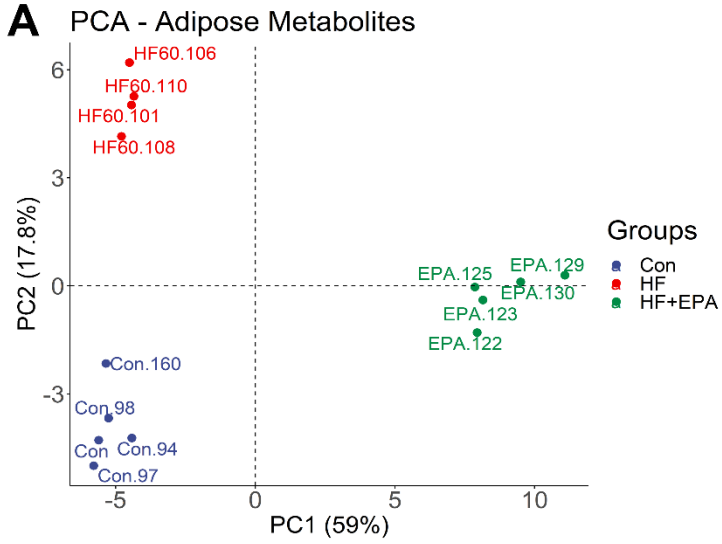

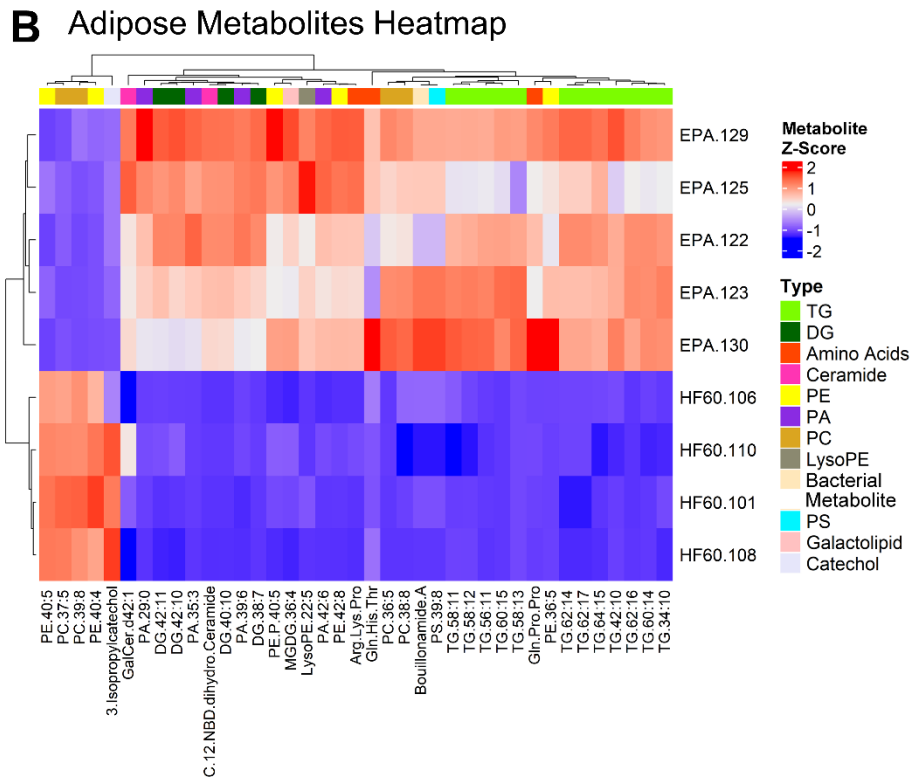

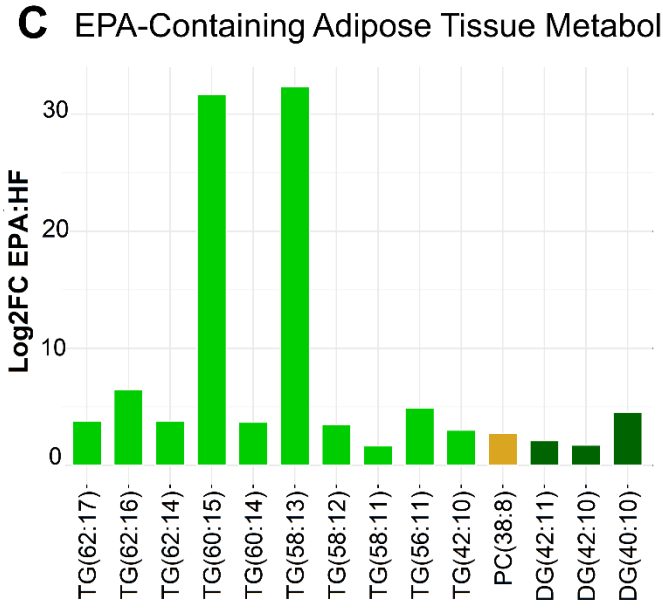

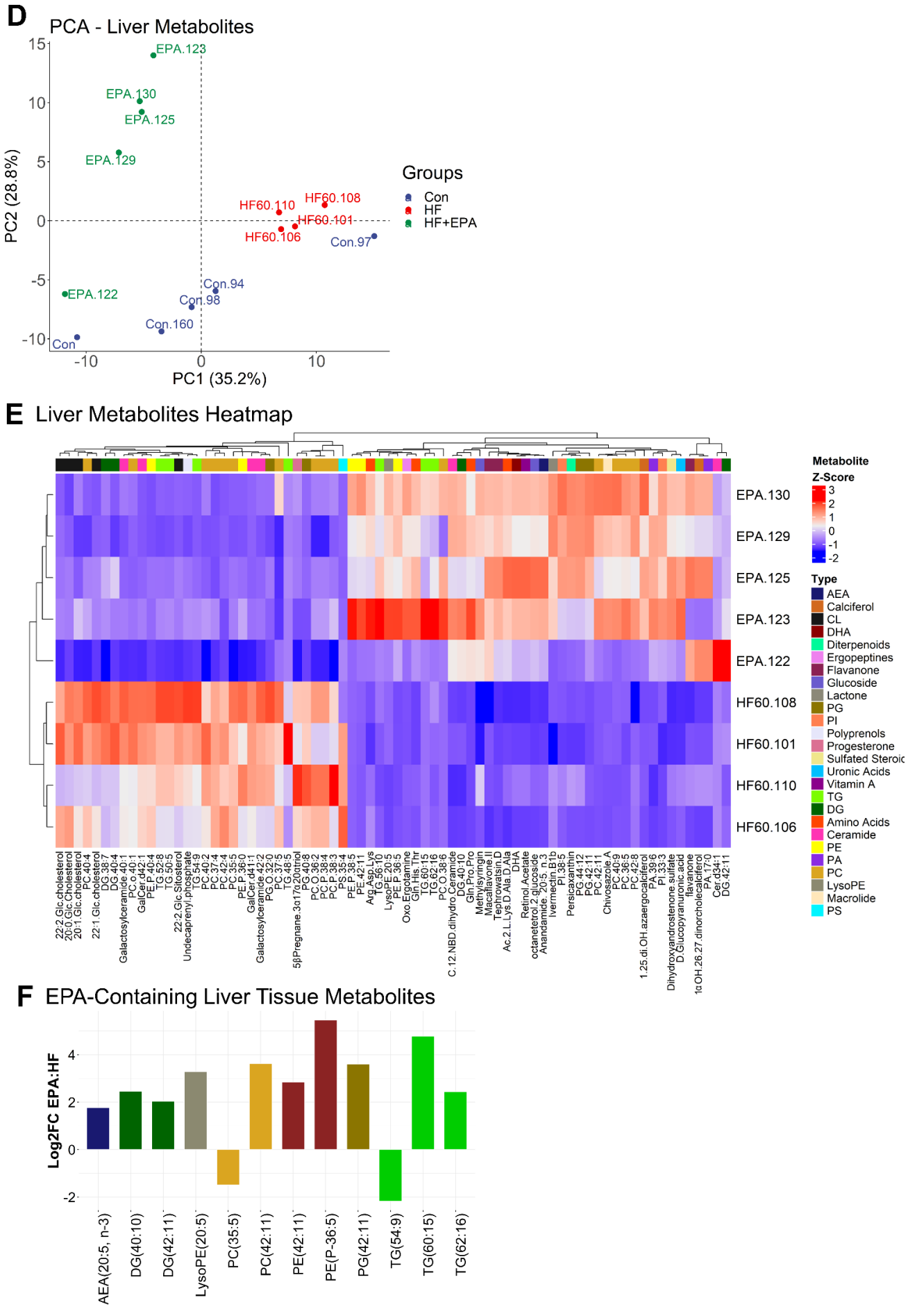

Figure 6

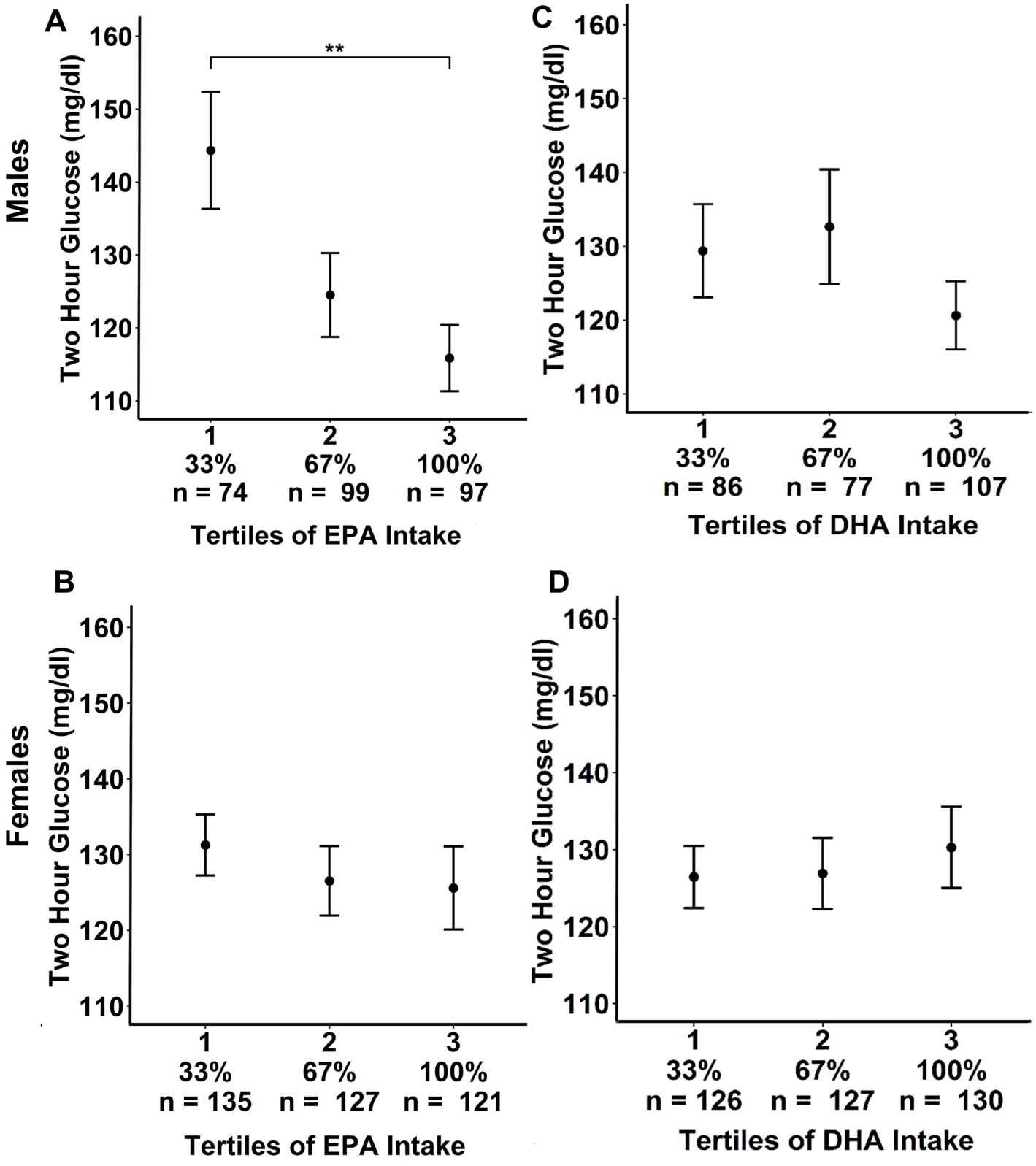

Figure 7

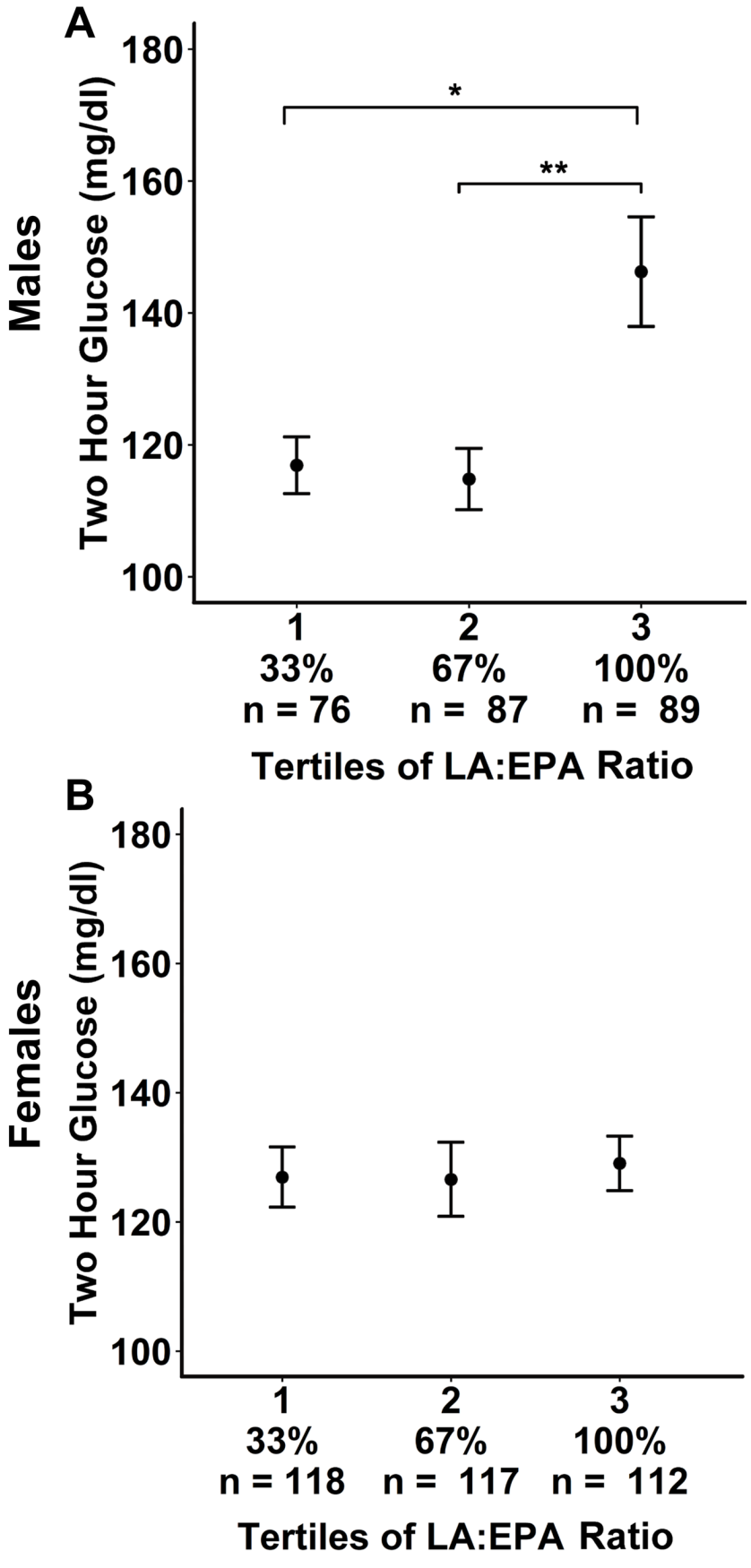

Figure 8

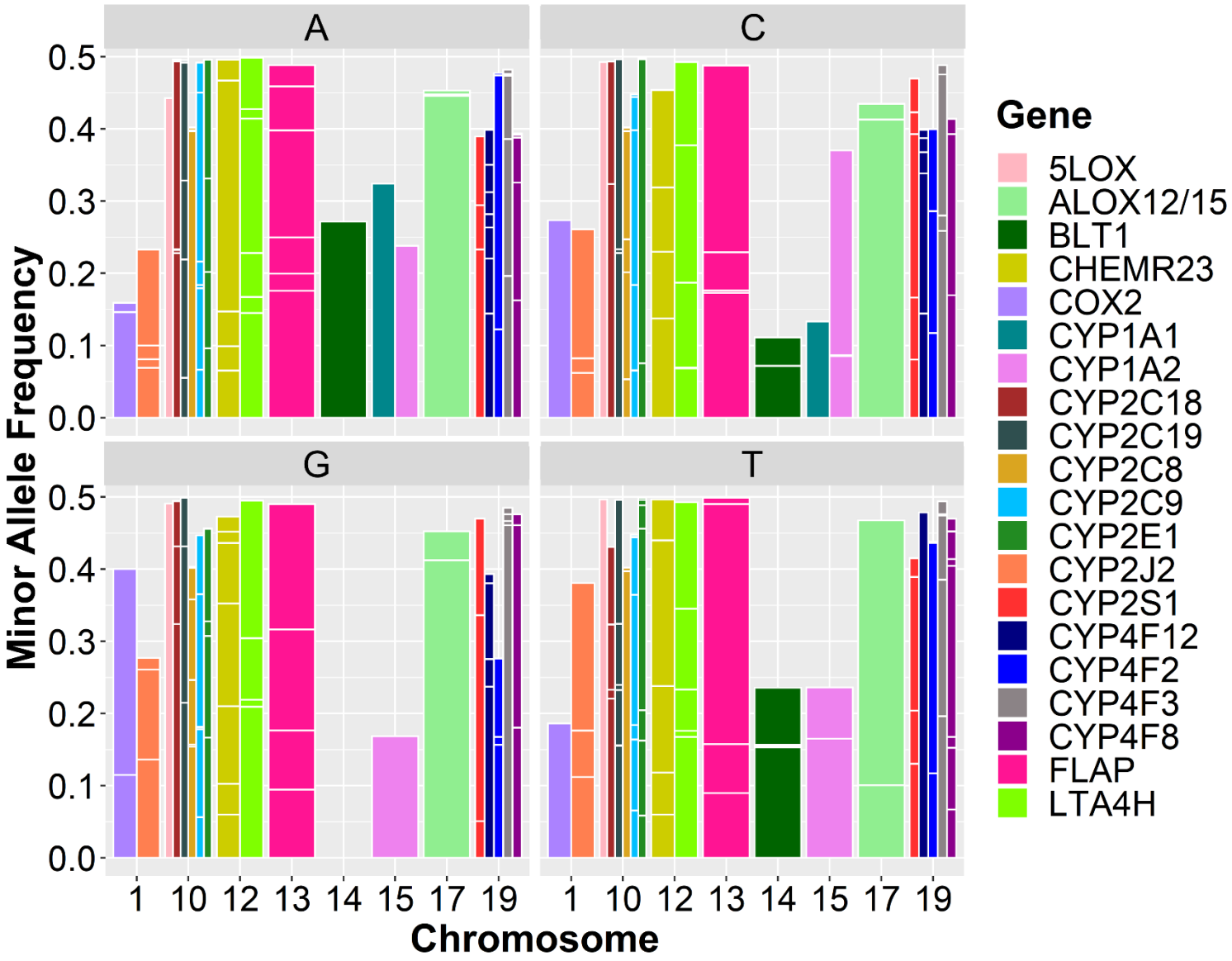

Figure 9